THE JOURNAL OF PHYSICAL CHEMISTRY C

Article

pubs.acs.org/JPCC

Carrier Transport in PbS and PbSe QD Films Measured by Photoluminescence Quenching

Jing Zhang,[‡] Jason Tolentino,[§] E. Ryan Smith,[†] Jianbing Zhang,[∥] Matthew C. Beard,[†] Arthur J. Nozik,[†,‡] Matt Law,[§] and Justin C. Johnson*[,†]

[†]National Renewable Energy Laboratory, 15013 Denver West Pkwy, Golden, Colorado 80401, United States

[‡]Department of Chemistry and Biochemistry, University of Colorado, Boulder, Colorado 80301, United States

[§]Department of Chemistry, University of California, Irvine, California 92697, United States

[∥]School of Optical and Electronic Information, Huazhong University of Science and Technology, 1037 Luoyu Road, Wuhan, Hubei 430074, China

Supporting Information

ABSTRACT: The temperature-dependent quantum yield of photoluminescence (PL) has been measured in films of various sizes of PbS and PbSe quantum dots (QDs) capped with alkanedithiol ligands with lengths varying from 4 to 20 Å. We demonstrate that PL within QD films can provide information about transport in a regime that is relevant to solar photoconversion. The ligand-length dependent PL quenching reveals behavior similar to that of ligand-length dependent carrier mobility determined from field-effect transistor (FET) measurements in the dark. The data are described by a model in which band tail luminescence is quenched upon thermal activation by charge separation and hopping followed by nonradiative recombination. We extract the tunneling parameter β and find values of 1.1 ± 0.2 Å^{-1} except for a value of 0.7 for the smallest QD sample. Changes in the transport mechanism may be due to unique surface faceting or QD-ligand coupling that occurs in small QDs. Furthermore, we compare all-organic capped PbS QD films with those infilled by Al_2O_3, discovering a surprisingly small value of β less than 0.3 for the latter, which may be related to a graded potential barrier because of amorphous Al_2O_3 at the QD surface or interfacial chemistry inherent in the atomic layer deposition process.

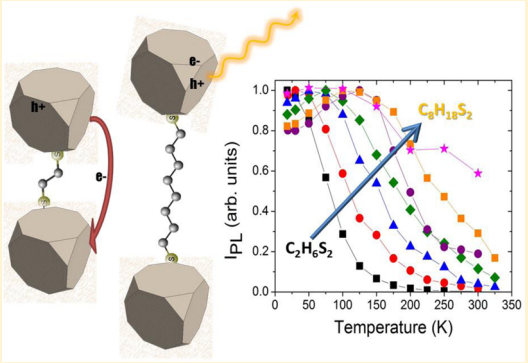

INTRODUCTION

The speed and efficiency of charge transport in quantum dot (QD) solids has improved dramatically in recent years. Field-effect transistor (FET) mobilities of >1 cm^2 V^{-1} s^{-1} are now commonly reported, usually after inorganic ligand[1,2] and/or atomic layer deposition (ALD) treatments.[3] Infilling QD films with an insulator has been previously shown to lead to increased long-term stability toward oxidation and improved mobilities, possibly due to trap state passivation.[4] However, the origin of the high mobility with respect to possible transport mechanisms has not been elucidated. It is believed that in disordered QD films that retain strong quantum confinement, sequential phonon-assisted tunneling of carriers between nearest-neighbor QDs dominates transport near room temperature. Mobilities less than about 10 cm^2 V^{-1} s^{-1} can be explained by such a mechanism.[5] Higher mobilities likely require communication between QDs that induces delocalization and possibly miniband formation.[6] The distance between QDs and the composition of the surrounding matrix are key parameters for determining the average tunneling rate of charges between two QDs, expressed as $\Gamma = \Gamma_0 \exp(-0.865\beta d) \exp(-E_a/k_BT)$.[7] Here, β is the decay constant of the wave function in the matrix material, d is the average edge-to-edge distance between QDs, E_a is an activation energy, k_B is Boltzmann's constant, and T is temperature. FET measurements that extracted the mobility of charge carriers in 6 nm PbSe QDs agreed with the expected exponential falloff in Γ with d, resulting in $\beta \sim 1.1$ Å^{-1} for alkanedithiol ligands. The parameter β can be estimated for an assumed square potential:[8] $\beta = (2m^*E_{barrier}/\hbar^2)^{1/2}$, in which $E_{barrier}$ is defined as the energy difference between the LUMO of the saturated hydrocarbon chains[9] and the conduction band of the QDs, and m^* is the electron effective mass (a similar formulation can be made for holes). If the intervening medium plays a role in charge transfer, models derived from superexchange[10] have often been invoked, and for QDs surrounded by a matrix with low lying electronic states, one might expect a considerable modification to the model of β derived using the Wentzel–Kramers–Brillouin (WKB) approximation.

Received: April 30, 2014
Revised: June 11, 2014
Published: June 27, 2014

dx.doi.org/10.1021/jp504240u | J. Phys. Chem. C 2014, 118, 16228–16235

While providing a measure of carrier mobility, FET measurements generally probe only 1−2 monolayers of QDs near the gate electrode and may be insensitive to trap states that become occupied upon gate biasing. Thus, complementary measurements of β that can be made under weak light excitation and little or no bias to ensure that occupation of electronic states throughout the bulk of the film is similar to that in a photovoltaic device would provide valuable new information. Photoluminescence (PL) of colloidal QDs is often used as an indicator of sample quality, and can usually be interpreted as radiative electron−hole (quantum-confined exciton) recombination when QDs are electronically isolated from each other.[11] Charge traps and resulting trapping/detrapping dynamics can play a significant role in carrier transport, especially for samples with surface states.[12,13] Surface states resulting from nonstoichiometry due to lattice termination have been characterized by their temperature-dependent PL, and their influence can be modulated by changing the composition of the QD surface via ligand exchange.[14] Defect states that result in nonradiative recombination centers can also be inferred via the temperature-dependent PL quenching that occurs as carriers overcome barriers to reach "dark" recombination centers through thermal activation. In QD films with relatively short organic or inorganic ligands, the dominant form of PL quenching is electron−hole separation and charge diffusion followed by nonradiative recombination.[15] In previous work, we interpreted size- and temperature-dependent PL quenching in terms of an exponential band tail model,[16] which faithfully reproduced both PL intensities and spectral profiles for films of PbS QDs capped with short ligands. In this model, photoexcited charges quickly relax to the band tail, where the charges are localized. They remain localized at low temperatures and recombine radiatively from the bottom of the density of states. At higher temperatures, the carriers can be activated in an Arrhenius fashion to states higher in the band tail that are delocalized, such that multiple trapping/detrapping events proceed, resulting in hopping transport. The energy demarcation between localization and delocalization, sometimes referred to as the mobility edge,[17,18] can be changed by QD size, ligands, and temperature, which redistributes electrons/holes within these states. Here we extend our previous work to make a direct connection between PL and charge transport by employing a series of ligands that increases the interdot distance but retains a consistent QD/ligand chemistry (i.e., thiolates) and matrix identity (i.e., alkanes). We show that the Arrhenius prefactor can be related in a simple way to the distance-dependent carrier tunneling rate.

Although demonstrations of high mobility and investigations of the transport mechanism in lead chalcogenide QD films have been carried out mostly on QDs with diameter greater than 5 nm, the most efficient QD solar cells have been fabricated from QDs with band gaps greater than 1 eV and confinement energies in excess of 0.5 eV,[19] corresponding to QD diameters < 4 nm. With a greater HOMO−LUMO splitting, the lowest exciton levels for small QDs are closer to electronic resonance with the surrounding matrix (e.g., the tunneling barrier is smaller). A close comparison with first-principles calculations is also possible with smaller QDs due to the lower computational cost of treating the necessary number of atoms.

EXPERIMENTAL METHODS

Sample Preparation. PbS and PbSe QDs were synthesized according to Hines et al.[20] and Yu et al.,[21] respectively, and kept air-free throughout synthesis, washing, and experiments. The films were either spin-cast in the case of untreated films (oleate-capped) or dip-coated from 1 mM solutions of the particular alkanedithiol in acetonitrile. The number of dipping cycles varied with the ligand from about 15 to about 30. The QD dipping solution was hexane and contained roughly 20 mg/mL of QDs. The optical density at the lowest exciton peak was typically 0.1. Sapphire was used as a substrate due to its superior infrared transmission and high thermal conductivity, although experiments performed with films cast on glass produced similar results. Absorption spectra were collected on a Shimadzu UV−vis−NIR spectrometer. The half-width at half-maximum OD was recorded for the lowest exciton absorption since for the smallest QD samples the full width was not resolved.

Photoluminescence Measurements. PL quantum yield measurements were performed on drop-cast films in an integrating sphere with either a 750 or 840 nm light-emitting diode as the excitation source and a cooled InGaAs photodiode as the detector. The films were air exposed for a few minutes during the experiment, but the Φ_{PL} for untreated PbS QDs was found to be stable during that period.

For temperature-dependent PL experiments, the 2 mm thick substrates were sealed in a 1 in diameter Cu holder with a Viton o-ring sandwiched between the substrate with the QD film and a blank sapphire substrate. The holder was sealed in the He glovebox and placed in a closed loop He flow cryostat (18−325 K) fitted with sapphire windows that was evacuated to 1×10^{-4} Torr. The sample was cooled to 18 K and then heated slowly in 20 K steps, with an equilibration time of 10 min at each temperature. Collecting PL spectra during cooling instead of heating produced the same results. The 514 nm line of an Ar-ion laser was used to excite the sample, with a beam size of approximately 2.5 mm and power roughly 30 mW. Each spectrum required roughly 1 min of exposure time. Experiments on some samples were performed at several powers (up to 100 mW) with no clear change in PL quenching behavior. The excitation beam was modulated at 500 Hz, and the sample emission was routed through a monochromator with a 300 groove/mm grating blazed at 1250 nm. A dual, balanced Ge photodiode was used in concert with a lock-in amplifier to detect the signal. The spectral sensitivity of the entire system was determined with a calibrated tungsten lamp, and PL spectra were corrected accordingly.

Atomic Layer Deposition. For atomic layer deposition infilling and overcoating, amorphous Al_2O_3 was deposited in a homemade continuous wave ALD system inside a glovebox using trimethylaluminum (TMA) and water (H_2O) at a substrate temperature of 27 °C and an operating pressure of 84−87 mTorr. Pulse and purge times for TMA were 20 ms and 60 s, respectively. Pulse and purge times for H_2O were 40 ms and 120 s, respectively.

Fabrication of QD Films for Field-Effect Measurements and Atomic Layer Deposition Infilling. PbS NC films were dip coated in a layer-by-layer fashion with a mechanical dip coater mounted inside an air-free glovebox. The substrates (prepatterned FET substrates or sapphire), cleaned by sonication in acetone and isopropanol, were dipped into a 2 mg mL^{-1} solution of QDs in dry hexane and then a 1 mM solution of the appropriate alkanedithiols in dry acetonitrile. We fabricated films with thicknesses in the range of 30−100 nm (thin for FETs and thicker for PL).

RESULTS AND DISCUSSION

In Figure 1 we show PL spectra versus temperature (18−325 K) for films of 3.8 nm PbS QDs treated with 1,2-ethanedithiol

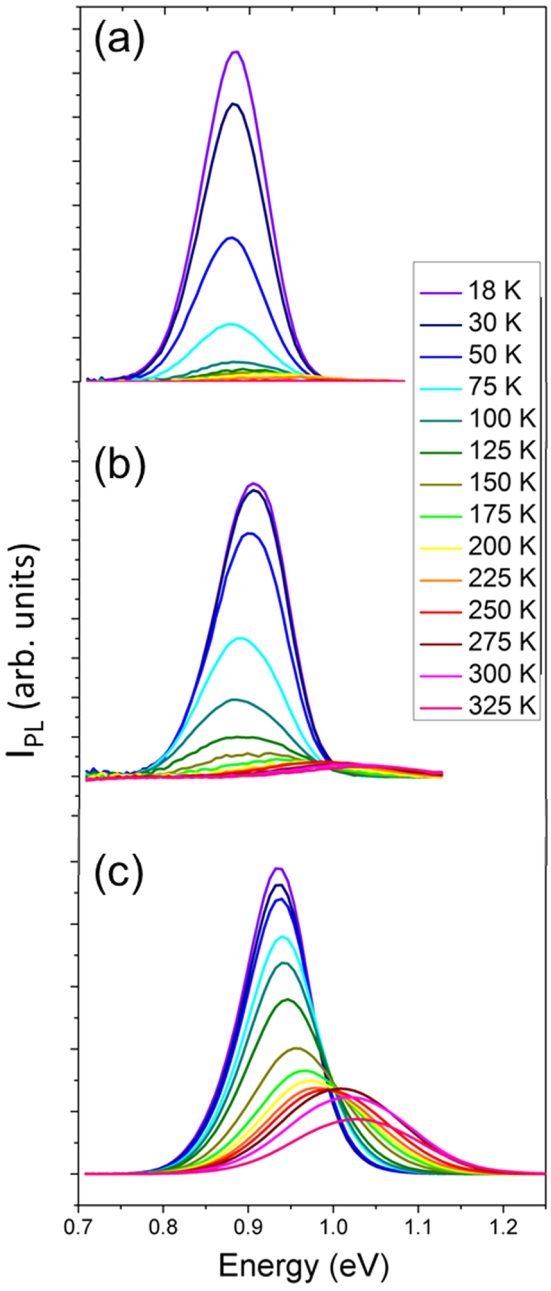

Figure 1. PL spectra for 3.8 nm PbS QD films treated with (a) EDT, (b) BuDT, or (c) ODT.

(EDT, Figure 1a), 1,4-butanedithiol (BuDT, Figure 1b), or 1,8-octanedithiol (ODT, Figure 1c). For EDT-treated films, an initial red shift is observed as the temperature is raised, consistent with activation of carriers into states closer to the mobility edge such that PL only arises from carriers that reside deeper in the band tails. The blue shift seen at higher temperatures is assigned to band gap widening for PbS[22] accounting for ∼20 meV of the shift[15] and redistribution of carriers to higher energy states responsible for the remainder. The blue shift occurs throughout the temperature range but is only evident at high temperatures when the deeper band tail emission is strongly quenched. The PL from ligand-exchanged samples was often too low to be quantified at room temperature, where absolute Φ_{PL} measurements were performed. Thus, Φ_{PL} of an oleate-capped QD film of each size was determined in an integrating sphere at 295 K, followed by a measurement of a reference spectrum collected in the temperature-dependent PL apparatus. The reference spectrum at room temperature was compared with spectra obtained from ligand-exchanged films at lower temperatures where emission was measurable in order to estimate Φ_{PL} at low temperature.

For PbSe QDs, the measured variation in Φ_{PL} was considerably larger than for PbS QDs, likely due to the particular sensitivity of PbSe to surface oxidation,[12,23] which can occur in the few minutes necessary to perform the integrating sphere measurements. We therefore could not reliably quantify integrated PL versus temperature for PbSe on an absolute scale. For PbS QDs at 18 K, Φ_{PL} is similar to that of uncoupled QDs in solution: 2−40% depending on QD size and ligand length (Table 1), which is calculated assuming length of 1.25 Å per sp^3

Table 1. Φ_{PL} for Various PbS QD Films at 18 K

treatment	nominal ligand length/ angstroms	2.3 nm Φ_{PL}	2.9 nm Φ_{PL}	3.8 nm Φ_{PL}	3.8 nm + ALD Φ_{PL}
none (oleic acid capped)	19.70	0.36	0.30	0.18	--
1,2-ethanedithiol (EDT)	4.25	0.039	0.11	0.021	0.016
1,3-propanedithiol (PrDT)	5.50	0.080	0.04	0.022	0.0031
1,4-butanedithiol (BuDT)	6.75	0.13	0.22	0.019	--
1,5-pentanedithiol (PeDT)	8.00	0.28	0.36	0.054	--
1,6-hexanedithiol (HDT)	9.25	0.29	0.37	0.074	0.03
1,8-octanedithiol (ODT)	11.75	0.32	0.36	0.13	--

C−C bond (1.54 Å bond length and tetrahedral angle of 109.5°). Φ_{PL} increases for smaller oleate-capped QDs, consistent with previous results that were explained by the energy dependence of likely nonradiative transitions, including both trapping in deep levels and energy transfer to ligands.[24,25]

Figure 2 displays the integrated PL intensity and peak energy versus ligand treatment and temperature for films of 2.9 nm PbS QDs (Figure 2a,b) and 2.5 nm PbSe QDs (Figure 2c,d). The behavior of PbS and PbSe QDs is qualitatively similar. There is an initial red shift with increasing temperature with a magnitude depending on ligand length−shorter ligands have a larger shift. The red shift is also QD size-dependent: ∼50 meV for 2.9 nm (Figure 2a) and ∼10 meV for 3.8 nm PbS QDs exchanged with EDT (Figure 1a). Concomitant with the reduction in red shift with increased QD size is a lowering of the temperature at which 50% PL quenching occurs, from 150 K for 2.3 nm PbS QDs capped with EDT (data not shown) to 50 K for the corresponding 3.8 nm QD film (Figure 1a). As the emission becomes strongly quenched at higher temperatures, the PL peak blueshifts by up to ∼80 meV from its minimum value to the position at room temperature.

In order to analyze the data in more detail, we derive a kinetic model that accounts for the expected routes of decay of the photoexcited carriers, including (1) radiative recombination

dx.doi.org/10.1021/jp504240u | J. Phys. Chem. C 2014, 118, 16228−16235

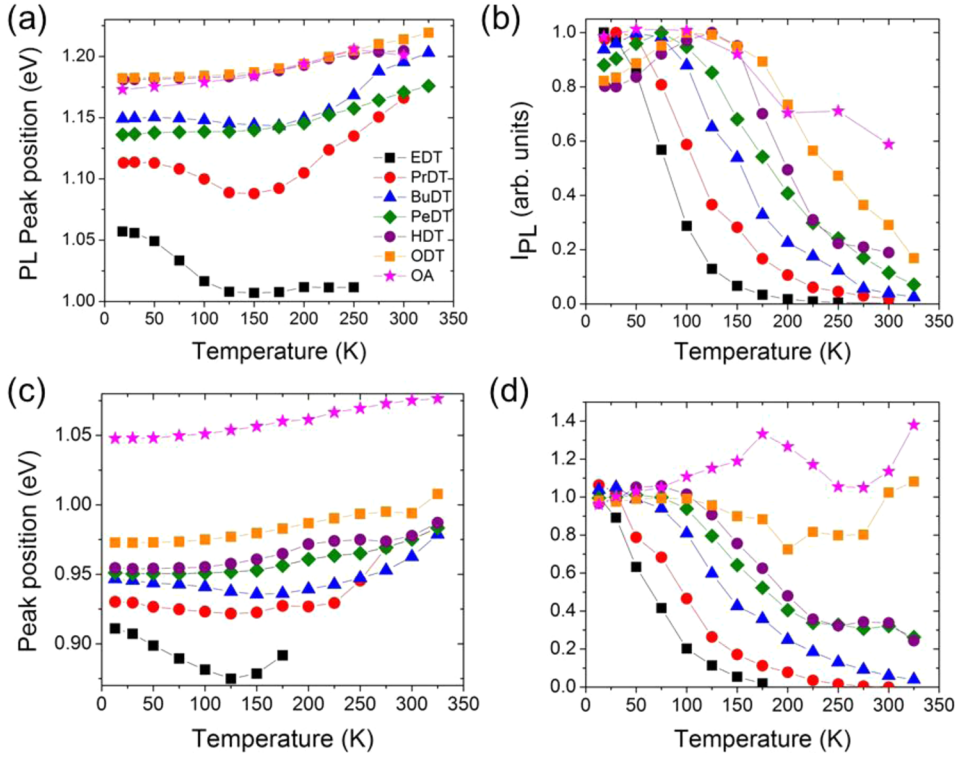

Figure 2. PL peak position and integrated PL intensity for (a,b) 2.9 nm PbS QDs and (c,d) 2.5 nm PbSe QDs.

from the bottom of the band; (2) nonradiative decay associated with carriers localized in individual QDs; and (3) carrier separation and diffusion leading to nonradiative decay at recombination sites. If we assume for simplicity that each of the rates is linear in light intensity, then Φ_{PL} can be described in terms of competing radiative and nonradiative processes:[26]

$$\Phi_{PL}(T) = \frac{k_{RR}}{k_{RR} + \sum k_{NR}} \tag{1}$$

where k_{RR} is the radiative recombination rate constant (corresponding to process (1)) and Σk_{NR} is the sum of various nonradiative recombination rate constants that in the following discussion we separate into temperature-independent (k_{NR}, process 2), and temperature-dependent (k_{CT}, process 3). As discussed above, when d is reduced, the PL quenching occurs at a lower temperature, which is consistent with diffusion-limited recombination. The most general form of the temperature-dependent hopping rate constant is

$$k_{CT}(T) = \alpha \exp\left(-\left(\frac{T*}{T}\right)^{\nu}\right) \tag{2}$$

which includes an attempt frequency α, an exponent ν, and a characteristic temperature $T*$. When $\nu = 1$, the nearest-neighbor hopping (NNH) transport regime is active, and $T*$ is expressed as an activation energy E_a. When $\nu = 0.5$, the Efros–Shklovskii variable range hopping (ES VRH) transport mechanism is dominant, while for $\nu = 0.25$ the Mott VRH regime applies.[7] The PL data sets do not afford adequate signal-to-noise ratios to determine the transport regime unequivocally. We assume that NNH is primarily responsible for the PL quenching, and further discussion of transport regimes can be found in the Supporting Information. We also assume that PL quenching is dominated by minority carriers (electrons) since previous studies have revealed p-type behavior for thiolate-capped PbS and PbSe QD films.[27]

With the additional assumption that k_{RR} is not strongly temperature dependent,[28] Φ_{PL} becomes

$$\Phi_{PL}(T) = \frac{k_{RR}}{k_{RR} + k_{CT}(T) + k_{NR}} = \frac{1}{1 + \frac{\alpha}{k_{RR}} e^{-\left(\frac{E_a}{k_B T}\right)} + k_{NR}/k_{RR}} \tag{3}$$

An example of a fit of eq 3 to the $\Phi_{PL}(T)$ data is shown in Figure 3 for 2.9 nm PbS QDs in various films.

In order to reduce the number of free parameters in fits with eq 3, we explored making some variables global in data sets of the same QD size but different length ligand. Fits in which E_a was made global among all $\Phi_{PL}(T)$ curves were superior to fits in which α was a global variable (Figure S1). This is most clearly seen for large d in which the curvature of $I_{PL}(T)$ near the

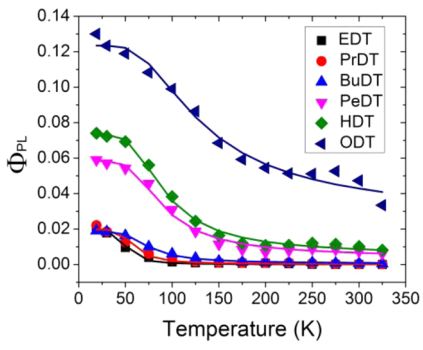

Figure 3. Simultaneous fit of eq 3 of temperature-dependent PL for films of 2.9 nm PbS QDs following alkanedithiol treatments.

dx.doi.org/10.1021/jp504240u | J. Phys. Chem. C 2014, 118, 16228–16235

Table 2. Lowest Exciton Peak Room Temperature Absorption Width ($fwhm_{abs}$), PL Peak Width ($fwhm_{PL}$) at 18K, Site Energy Disorder (E_D), Coulomb Charging Energy (E_C), and Best-Fit Values of β, k_{NR}, and E_a for Three PbS QD Films[a]

peak abs/eV	$fwhm_{abs}$/eV	$fwhm_{PL}$/eV	E_D/meV	E_C/meV	E_a/meV (ν = 1)	k_{NR} (sec^{-1})	β/Å^{-1}
1.69	266	185	112	63	96	3.5×10^6	0.7 ± 0.06
1.39	154	145	66	45	127	6.1×10^6	1.1 ± 0.18
1.12	132	90	56	27	34	1.5×10^7	0.9 ± 0.08

[a] E_C, $FWHM_{PL}$, and k_{NR} are determined for EDT capping.

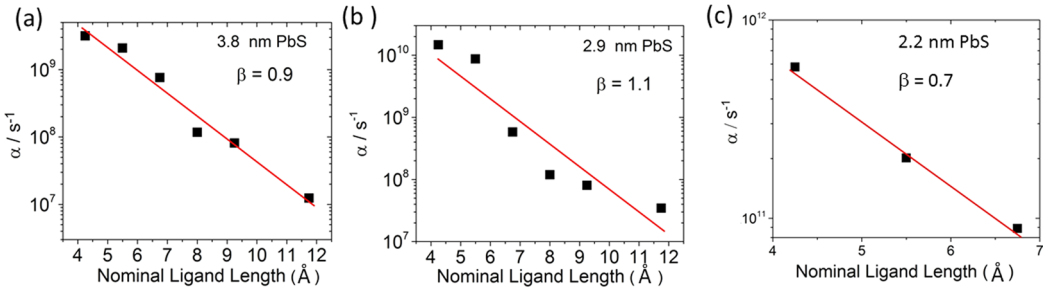

Figure 4. Frequency factor α versus QD separation for 3.8 and 2.9, and 2.3 nm PbS QDs films.

quenching temperature is noticeably reduced, which can only be fitted properly if α changes with d. When E_a and α were both allowed to vary, the dependence of α on ligand length was retained while there was no trend for E_a. If the Coulomb charging energy E_C were to dictate the dependence of E_a on d, then $E_a \propto d^1$, but the lack of a clear dependence implies that E_C is not the primary source of the potential barrier to hopping in these samples. Table 2 displays various fitted and calculated parameters for three sets of PbS QD samples. Here we have assumed a k_{RR} value of 3×10^5 s^{-1}.[29] The value of k_{NR} is shown only for EDT capping but scales according to Φ_{PL} (18K) for other ligands (Figure S3). Similar data for the PbSe QD samples are found in Table S1 and Figure S2.

We connect the prefactor α in $\Phi_{PL}(T)$ to the first term in the Miller–Abrahams equation[30] also used for determination of β from FET measurements:[9]

$$\alpha \propto e^{-0.865\beta d} \quad (4)$$

Plots of α versus d on a semilog scale for the two larger PbS QD sizes (Figure 4a,b) reveal approximately linear trends with extracted β values ~1 Å^{-1}, similar to FET results.[9] There are small deviations from linearity through the alkanedithiol series, which likely arise from the assumption that the interparticle spacing d is equal to the calculated ligand length. Ligand conformations that allow for bidentate binding[31] or varying degrees of interdigitation could give rise to the nonlinearity, which has been observed in other determinations of β for treated QD films[9,15] and in molecular conductance studies that employed alkanedithiol ligands.[32] The maximum pre-exponential factor α_0 (α extrapolated to $d = 0$) is ~1×10^{12} s^{-1}, 1×10^{13} s^{-1}, and 3×10^{12} s^{-1} for 3.8, 2.9, and 2.3 nm PbS QDs, respectively. Using α values for EDT-exchanged films in the Einstein–Smoluchowski relation ($\mu = (e/2kT)d^2\alpha$) results in mobilities ranging from 5×10^{-4} to 4×10^{-2} cm^2 V^{-1} s^{-1} at room temperature, consistent with the magnitude of electron mobilities determined by FET measurements performed on similar films (Figure S4).

For 2.2 nm PbS QD films (Figure 4c), full PL quenching does not occur until at or above room temperature for ligands longer than BuDT, and heating above 325 K was not performed since film rearrangement or sintering may produce uncontrolled effects on the PL signal. Further uncertainty arises from the fact that the $I_{PL}(T)$ curves have a peak at intermediate temperatures for smaller QDs, especially for longer ligands. Thus, we restricted our analysis to EDT, PrDT, and BuDT for this QD size, which gives $\beta \sim 0.7$ Å^{-1}. For QDs with diameters larger than 4 nm, the PL was too weak for a proper analysis, thus it was not possible to determine a value of β.

In Figure 5 are shown normalized $\Phi_{PL}(T)$ curves for 3.8 nm PbS QD films infilled with Al_2O_3.[33] The quenching behavior

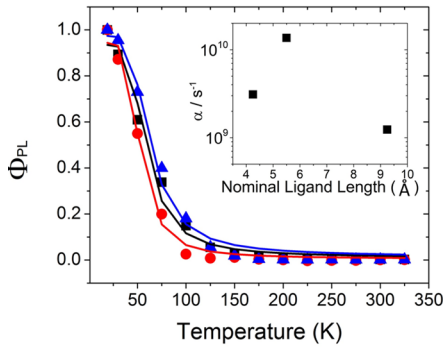

Figure 5. PL of Al_2O_3-infilled 3.8 nm PbS QD film previously treated with alkanedithiols. Φ_{PL} is normalized to unity at 18 K for each sample. Inset: α vs ligand length.

remains essentially the same for each of the three different length ligand treatments. The Φ_{PL} values at 18 K (Table 1) are significantly smaller than those observed for non-ALD infilled films, suggesting surface chemistry that enhances k_{NR} or more facile charge separation at low temperature. The data were fitted with eq 3 and the resulting α versus d trend is shown in the inset.

Unlike in high-quality bulk semiconductors,[34] the room temperature PL for high-mobility QD films at open circuit is low due to the dominance of nonradiative over radiative recombination. Thus, the most informative aspect of the steady-state PL from coupled QD films is its temperature dependence, rather than the absolute value of Φ_{PL} at room temperature. However, relatively high values of Φ_{PL} at low temperature and the trend with ligand length prove that the PL

dx.doi.org/10.1021/jp504240u | J. Phys. Chem. C 2014, 118, 16228–16235

is not emitted from a small subset of QDs disconnected from the relevant events of charge separation and diffusion. The trend of larger Φ_{PL} with smaller QD size has been previously observed in solution and discussed in terms of the energy gap law that dictates nonradiative decay rates, which should also be relevant here.[24] Surface faceting and stoichiometry are additional size-dependent effects that could influence Φ_{PL}.[35,14] The amount of surface chalcogen increases for larger QDs[36] and has been previously implicated in poor emission yields of CdSe and PbSe.[37,38] The trend of lower Φ_{PL} with decreased ligand length at low temperature (Table 1) likely results from two factors: (1) a different ligand packing geometry leading to increased density of QD-ligand bonds and a higher surface anion content, or (2) an increase in interdot coupling that facilitates exciton dissociation with minimal thermal activation. The trend of Φ_{PL} versus d at 18 K matches that of the PL peak shift with d (Figure S3), which suggests that interdot coupling inferred from PL red-shifting is a dominant factor.

Although the barrier height $E_{barrier}$ to carrier tunneling is primarily determined by the electronic structure of the matrix, the activation energy E_a is affected by other factors. In temperature-dependent dark conductivity measurements, E_a has been asserted to depend on the distribution of lowest exciton energies in the QD ensemble and/or the Coulomb charging energy E_C for charge transfer between QDs.[39] The $fwhm_{abs,}$ of the lowest exciton absorption, which is one measure of energy disorder, varies significantly through our sample series (Table 2). The site energy disorder, E_D in Table 2 and Table S1, is calculated using $E_D = fwhm_{abs}/2(2 \ln 2)^{1/2}$, which is the standard deviation of the Gaussian distribution of lowest exciton energies. We find at best a weak correlation between the size-dependent trends of E_D and E_a. The Coulomb charging energy E_C should be proportional to 1/diameter, and we show in Table 2 calculated values using the formalism as in ref 9. The magnitude of E_C is smaller than that of E_D but coincidentally follows a similar trend. The lack of a clear dependence of E_a on d in the fits suggests that the contribution from E_C is minor. Other QD size-dependent contributions to E_a could include increasing bond length disorder due to changing surface to volume ratio and a higher degree of "charging" (i.e., long-lived trapped carriers) due to the presence of higher energy facets, both of which could deepen the band tail and increase E_a.[40] Ligand phase transitions were also previously asserted to play a role in temperature-dependent quenching behavior, which would potentially modulate E_a.[41]

β measured by PL quenching is 1.1 ± 0.2 $Å^{-1}$ for the two larger PbS and PbSe QD samples, in agreement with measured FET mobility vs ligand length for PbSe QDs for both the electron and the hole. The lower β value of ~0.7 $Å^{-1}$ for the smallest PbS QD sample implies a size-dependent barrier for carrier tunneling. The very large confinement energy (>1 eV) for the smallest QDs could have consequences for both $E_{barrier}$ and the probability of mixing between QD and ligand states. The additional 0.3 eV in confinement energy for the 2.3 nm QDs will result mostly in a rise in the conduction band edge,[42,43] although unless the barrier for the larger QDs is significantly less than the 1.6 eV previously estimated, the effect cannot account for such a large decrease in β.

The possibility of increased interaction between band edge states and ligand orbitals is intriguing but difficult to test. The effect of mixing may be to smooth the abrupt square potential barrier that is assumed in the WKB model of β.[44] Relatively fast charge transfer from PbS and PbSe QDs to ligands is well-established;[45−47] however, in most cases the acceptor is designed to capture charge rather than serve as a conduit between QDs. It was suggested that the reason for the anomalously low 1.6 eV barrier for carrier tunneling in PbSe QDs capped with alkanethiols was QD-ligand mixing.[9] For that size, the confinement energy was only 0.4 eV, ~1 eV smaller than that of the PbS QDs studied here. Thus, if mixing occurs for larger QDs, it is likely to be much stronger for smaller QDs whose lowest exciton levels are closer to resonance with ligand levels. Measurements of transient photoconductivity performed on films composed of PbSe QDs treated with different length alkyldiamines revealed β of 0.57 A^{-1}.[48] Mixing with ligand states was suggested as a reason for the lower than expected β value, but no definitive conclusions were drawn. Through time-resolved PL measurements Choi et al. also reported a relatively low value of β = 0.26 A^{-1} for PbS QDs capped with dithiols, although the linker chains consisted of benzene units rather than saturated chains.[49] More recently, Scheele et al. claimed a resonant alignment between the valence band of 9.8 nm PbS QDs and a tetrathifulvalenetetracarboxylate ligand.[50] Anomalously high FET mobilites for the measured interdot spacing as well as XPS data and atomistic calculations supported the notion that transport was ligand-assisted. Tailored inorganic ligands were not employed here, but are even more likely to serve as active participants in charge transport.[1,51]

Since surface faceting changes with QD size, it is possible that interactions between specific facets are more strongly engendered for small QDs. For example, it has been shown through DFT calculations[52] that when coupling occurs via the (111) facet, which becomes more dominant in small PbS or PbSe QDs, the coupling energy is attenuated more weakly with interdot spacing than similar coupling via the (100) facet. Local QD alignment along the (111) facets, or even some degree of necking, may facilitate the lower barrier to charge transfer.

PbS QD films infilled with alumina exhibit increased electron FET mobility (from ~10^{-3} to ~10^{-2} cm^2 V^{-1} s^{-1} for EDT treated QDs, Figure S4) compared with noninfilled films, but a β of less than 0.3. The similar $I_{PL}(T)$ profiles after ALD suggest that PL quenching occurs by the same mechanism as in noninfilled films. If the expression $\beta = (2m^*E_{barrier}/\hbar^2)^{1/2}$ holds, the much smaller value of β for alumina-infilled films would suggest an order of magnitude decrease in the product of the tunneling barrier height and the carrier effective mass. However, the large band gap of crystalline Al_2O_3 (~6 eV) should result in $E_{barrier}$ greater than 2 eV and thus not much smaller than that of the alkanedithiols, which also exhibited $E_{barrier}$ ~ 2 eV. Moreover, studies of ALD coating of Al_2O_3 on TiO_2 or SnO_2 revealed a β of about 1 $Å^{-1}$ for electron tunneling, with a barrier height similar to that expected for PbS QDs.[53] One possibility is that amorphous Al_2O_3 material, with a band gap of 2.6−2.9 eV,[54] is formed at the surface of the QDs and may serve to smooth the potential barrier. Possible surface chemistry modifications including surface doping after ALD may also influence β but have not been studied systematically.

CONCLUSIONS

We have shown a clear correlation between PL quenching and previously reported field-effect mobility measurements for QD films with varying inter-QD spacing. For relatively large PbS QDs (diameter >2.5 nm), the data can be fitted with a model in which charge carriers tunnel between states on weakly coupled QDs with β ~ 1. For smaller QDs, the value of β is reduced, possibly due to effects related to the interaction between

particular surface facets or mixing with ligand states due to the large confinement energy. Alumina-infilled 3.8 nm PbS QD films exhibit an unusually small β, which cannot be explained solely by the expected change in barrier height for crystalline Al_2O_3 compared with alkanedithiols. Our results show that utilizing steady-state PL to determine barriers to charge transport on QD films intended for solar photoconversion can reveal important trends that may complement information from electrical measurements.

■ ASSOCIATED CONTENT

Supporting Information

Discussion of transport regime, additional global fitting information, PL data and analysis for PbSe QDs, PL quantum yield and peak shift correlation, and FET measurements. This material is available free of charge via the Internet at http://pubs.acs.org.

■ AUTHOR INFORMATION

Corresponding Author

*Mailing address: NREL, 15013 Denver West Pkwy, Golden, CO 80401. Phone: 303-384-6190; e-mail: justin.johnson@nrel.gov.

Notes

The authors declare no competing financial interest.

■ ACKNOWLEDGMENTS

The authors gratefully acknowledge the Center for Advanced Solar Photophysics (CASP), an Energy Frontier Research Center sponsored by Basic Energy Sciences, U.S. Department of Energy. J.T. acknowledges support from an NSF Graduate Research Fellowship.

■ REFERENCES

(1) Lee, J. S.; Kovalenko, M. V.; Huang, J.; Chung, D. S.; Talapin, D. V. Band-Like Transport, High Electron Mobility and High Photoconductivity in All-Inorganic Nanocrystal Arrays. *Nat. Nanotechnol.* **2011**, *6*, 348−352.

(2) Choi, J. H.; Fafarman, A. T.; Oh, S. J.; Ko, D. K.; Kim, D. K.; Diroll, B. T.; Muramoto, S.; Gillen, J. G.; Murray, C. B.; Kagan, C. R. Bandlike Transport in Strongly Coupled and Doped Quantum Dot Solids: A Route to High-Performance Thin-Film Electronics. *Nano Lett.* **2012**, *12*, 2631−2638.

(3) Liu, Y.; Tolentino, J.; Gibbs, M.; Ihly, R.; Perkins, C. L.; Liu, Y.; Crawford, N.; Hemminger, J. C.; Law, M. PbSe Quantum Dot Field-Effect Transistors with Air-Stable Electron Mobilities above 7 $cm^2 V^{-1} s^{-1}$. *Nano Lett.* **2013**, *13*, 1578−1587.

(4) Liu, Y.; Gibbs, M.; Perkins, C. L.; Tolentino, J.; Zarghami, M. H.; Bustamante, J.; Law, M. Robust, Functional Nanocrystal Solids by Infilling with Atomic Layer Deposition. *Nano Lett.* **2011**, *11*, 5349−5355.

(5) Shabaev, A.; Efros, A. L.; Efros, A. L. Dark and Photo-Conductivity in Ordered Array of Nanocrystals. *Nano Lett.* **2013**, *13*, 5454−5461.

(6) Nozik, A. J. Spectroscopy and Hot Electron Relaxation Dynamics in Semiconductor Quantum Wells and Quantum Dots. *Annu. Rev. Phys. Chem.* **2001**, *52*, 193−231.

(7) Shklovskiĭ, B. I.; Efros, A. L. *Electronic Properties of Doped Semiconductors*; Springer-Verlag: Berlin/New York, 1984.

(8) Gurney, R. W.; Condon, E. U. *Phys. Rev.* **1929**, *33*, 127−140.

(9) Liu, Y.; Gibbs, M.; Puthussery, J.; Gaik, S.; Ihly, R.; Hillhouse, H. W.; Law, M. Dependence of Carrier Mobility on Nanocrystal Size and Ligand Length in PbSe Nanocrystal Solids. *Nano Lett.* **2010**, *10*, 1960−1969.

(10) Gray, H. B.; Winkler, J. R. Long-Range Electron Transfer. *Proc. Natl. Acad. Sci. U.S.A.* **2005**, *102*, 3534−3539.

(11) Dabbousi, B. O.; RodriguezViejo, J.; Mikulec, F. V.; Heine, J. R.; Mattoussi, H.; Ober, R.; Jensen, K. F.; Bawendi, M. G. (CdSe)ZnS Core-Shell Quantum Dots: Synthesis and Characterization of a Size Series of Highly Luminescent Nanocrystallites. *J. Phys. Chem. B* **1997**, *101*, 9463−9475.

(12) Chappell, H. E.; Hughes, B. K.; Beard, M. C.; Nozik, A. J.; Johnson, J. C. Emission Quenching in PbSe Quantum Dot Arrays by Short-Term Air Exposure. *J. Phys. Chem. Lett.* **2011**, *2*, 889−893.

(13) Nagpal, P.; Klimov, V. I. Role of Mid-Gap States in Charge Transport and Photoconductivity in Semiconductor Nanocrystal Films. *Nat. Commun.* **2011**, *2*, 486.

(14) Hughes, B. K.; Ruddy, D. A.; Blackburn, J. L.; Smith, D. K.; Bergren, M. R.; Nozik, A. J.; Johnson, J. C.; Beard, M. C. Control of PbSe Quantum Dot Surface Chemistry and Photophysics Using an Alkylselenide Ligand. *ACS Nano* **2012**, *6*, 5498−5506.

(15) Gao, J. B.; Johnson, J. C. Charge Trapping in Bright and Dark States of Coupled PbS Quantum Dot Films. *ACS Nano* **2012**, *6*, 3292−3303.

(16) Tsang, C.; Street, R. A. Recombination in Plasma-Deposited Amorphous Si−H - Luminescence Decay. *Phys. Rev. B* **1979**, *19*, 3027−3040.

(17) Werner, J.; Peisl, M. Exponential Band Tails in Polycrystalline Semiconductor Films. *Phys. Rev. B* **1985**, *31*, 6881−6883.

(18) Mott, N. The Mobility Edge since 1967. *J. Phys. C* **1987**, *20*, 3075−3102.

(19) Maraghechi, P.; et al. The Donor-Supply Electrode Enhances Performance in Colloidal Quantum Dot Solar Cells. *ACS Nano* **2013**, *7*, 6111−6116.

(20) Hines, M. A.; Scholes, G. D. Colloidal PbS Nanocrystals with Size-Tunable Near-Infrared Emission: Observation of Post-Synthesis Self-Narrowing of the Particle Size Distribution. *Adv. Mater.* **2003**, *15*, 1844−1849.

(21) Yu, W. W.; Falkner, J. C.; Shih, B. S.; Colvin, V. L. Preparation and Characterization of Monodisperse PbSe Semiconductor Nanocrystals in a Noncoordinating Solvent. *Chem. Mater.* **2004**, *16*, 3318−3322.

(22) Olkhovets, A.; Hsu, R. C.; Lipovskii, A.; Wise, F. W. Size-Dependent Temperature Variation of the Energy Gap in Lead-Salt Quantum Dots. *Phys. Rev. Lett.* **1998**, *81*, 3539−3542.

(23) Sykora, M.; Koposov, A. Y.; McGuire, J. A.; Schulze, R. K.; Tretiak, O.; Pietryga, J. M.; Klimov, V. I. Effect of Air Exposure on Surface Properties, Electronic Structure, and Carrier Relaxation in PbSe Nanocrystals. *ACS Nano* **2010**, *4*, 2021−2034.

(24) Semonin, O. E.; Johnson, J. C.; Luther, J. M.; Midgett, A. G.; Nozik, A. J.; Beard, M. C. Absolute Photoluminescence Quantum Yields of IR-26 Dye, PbS, and PbSe Quantum Dots. *J. Phys. Chem. Lett.* **2010**, *1*, 2445−2450.

(25) Moreels, I.; Justo, Y.; De Geyter, B.; Haustraete, K.; Martins, J. C.; Hens, Z. Size-Tunable, Bright, and Stable PbS Quantum Dots: A Surface Chemistry Study. *ACS Nano* **2011**, *5*, 2004−2012.

(26) Lakowicz, J. R. *Principles of Fluorescence Spectroscopy*, 2nd ed.; Kluwer Academic Publishers: New York, 1999.

(27) Luther, J. M.; Law, M.; Song, Q.; Perkins, C. L.; Beard, M. C.; Nozik, A. J. Structural, Optical and Electrical Properties of Self-Assembled Films of PbSe Nanocrystals Treated with 1,2-Ethanedithiol. *ACS Nano* **2008**, *2*, 271−280.

(28) Kigel, A.; Brumer, M.; Maikov, G.; Sashchiuk, A.; Lifshitz, E. The Ground-State Exciton Lifetime of PbSe Nanocrystal Quantum Dots. *Superlattice Microstruct.* **2009**, *46*, 272−276.

(29) Clark, S. W.; Harbold, J. M.; Wise, F. W. Resonant Energy Transfer in PbS Quantum Dots. *J. Phys. Chem. C* **2007**, *111*, 7302−7305.

(30) Miller, A.; Abrahams, E. *Phys. Rev. B* **1960**, *120*, 745−755.

(31) Joo, S. W.; Han, S. W.; Kim, K. Adsorption Characteristics of 1,3-Propanedithiol on Gold: Surface-Enhanced Raman Scattering and Ellipsometry Study. *J. Phys. Chem. B* **2000**, *104*, 6218−6224.

(32) Pires, E.; Macdonald, J. E.; Elliott, M. Chain Length and Temperature Dependence of Alkanedithiol Molecular Conductance under Ultra High Vacuum. *Nanoscale.* **2013**, *5*, 9397−9403.
(33) Ihly, R.; Tolentino, J.; Liu, Y.; Gibbs, M.; Law, M. The Photothermal Stability of Pbs Quantum Dot Solids. *ACS Nano* **2011**, *5*, 8175−8186.
(34) Miller, O. D.; Yablonovitch, E.; Kurtz, S. R. Strong Internal and External Luminescence as Solar Cells Approach the Shockley−Queisser Limit. *IEEE J. Photovolt.* **2012**, *2*, 303−311.
(35) Moreels, I.; Lambert, K.; De Muynck, D.; Vanhaecke, F.; Poelman, D.; Martins, J. C.; Allan, G.; Hens, Z. Composition and Size-Dependent Extinction Coefficient of Colloidal PbSe Quantum Dots. *Chem. Mater.* **2007**, *19*, 6101−6106.
(36) Petkov, V.; Moreels, I.; Hens, Z.; Ren, Y. PbSe Quantum Dots: Finite, Off-Stoichiometric, and Structurally Distorted. *Phys. Rev. B* **2010**, *81*, 241304.
(37) Bae, W. K.; Joo, J.; Padilha, L. A.; Won, J.; Lee, D. C.; Lin, Q. L.; Koh, W. K.; Luo, H. M.; Klimov, V. I.; Pietryga, J. M. Highly Effective Surface Passivation of PbSe Quantum Dots through Reaction with Molecular Chlorine. *J. Am. Chem. Soc.* **2012**, *134*, 20160−20168.
(38) Jasieniak, J.; Mulvaney, P. From Cd-Rich to Se-Rich - The Manipulation of CdSe Nanocrystal Surface Stoichiometry. *J. Am. Chem. Soc.* **2007**, *129*, 2841−2848.
(39) Kang, M. S.; Sahu, A.; Norris, D. J.; Frisbie, C. D. Size- and Temperature-Dependent Charge Transport in PbSe Nanocrystal Thin Films. *Nano Lett.* **2011**, *11*, 3887−3892.
(40) Erslev, P. T.; Chen, H. Y.; Gao, J. B.; Beard, M. C.; Frank, A. J.; van de Lagemaat, J.; Johnson, J. C.; Luther, J. M. Sharp Exponential Band Tails in Highly Disordered Lead Sulfide Quantum Dot Arrays. *Phys. Rev. B* **2012**, *86*, 155313.
(41) Nelson, G. A.; Zhu, X. Y. Reversible Surface Electronic Traps in PbS Quantum Dot Solids Induced by an Order−Disorder Phase Transition in Capping Molecules. *J. Am. Chem. Soc.* **2012**, *134*, 7592−7595.
(42) Jasieniak, J.; Califano, M.; Watkins, S. E. Size-Dependent Valence and Conduction Band-Edge Energies of Semiconductor Nanocrystals. *ACS Nano* **2011**, *5*, 5888−5902.
(43) Hyun, B. R.; Zhong, Y. W.; Bartnik, A. C.; Sun, L. F.; Abruna, H. D.; Wise, F. W.; Goodreau, J. D.; Matthews, J. R.; Leslie, T. M.; Borrelli, N. F. Electron Injection from Colloidal PbS Quantum Dots into Titanium Dioxide Nanoparticles. *ACS Nano* **2008**, *2*, 2206−2212.
(44) Wuelfing, W. P.; Green, S. J.; Pietron, J. J.; Cliffel, D. E.; Murray, R. W. Electronic Conductivity of Solid-State, Mixed-Valent, Monolayer-Protected Au Clusters. *J. Am. Chem. Soc.* **2000**, *122*, 11465−11472.
(45) Hyun, B. R.; Bartnik, A. C.; Lee, J. K.; Imoto, H.; Sun, L. F.; Choi, J. J.; Chujo, Y.; Hanrath, T.; Ober, C. K.; Wise, F. W. Role of Solvent Dielectric Properties on Charge Transfer from PbS Nanocrystals Molecules. *Nano Lett.* **2010**, *10*, 318−323.
(46) Knowles, K. E.; Peterson, M. D.; McPhail, M. R.; Weiss, E. A. Exciton Dissociation within Quantum Dot−Organic Complexes: Mechanisms, Use as a Probe of Interfacial Structure, and Applications. *J. Phys. Chem. C* **2013**, *117*, 10229−10243.
(47) Zhu, H. M.; Yang, Y.; Lian, T. Q. Multiexciton Annihilation and Dissociation in Quantum Confined Semiconductor Nanocrystals. *Acc. Chem. Res.* **2013**, *46*, 1270−1279.
(48) Gao, Y. N.; Aerts, M.; Sandeep, C. S. S.; Talgorn, E.; Savenije, T. J.; Kinge, S.; Siebbeles, L. D. A.; Houtepen, A. J. Photoconductivity of PbSe Quantum-Dot Solids: Dependence on Ligand Anchor Group and Length. *ACS Nano* **2012**, *6*, 9606−9614.
(49) Choi, J. J.; Luria, J.; Hyun, B. R.; Bartnik, A. C.; Sun, L. F.; Lim, Y. F.; Marohn, J. A.; Wise, F. W.; Hanrath, T. Photogenerated Exciton Dissociation in Highly Coupled Lead Salt Nanocrystal Assemblies. *Nano Lett.* **2010**, *10*, 1805−1811.
(50) Scheele, M.; Hanifi, D.; Zherebetskyy, D.; Chourou, S. T.; Axnanda, S.; Rancatore, B. J.; Thorkelsson, K.; Xu, T.; Liu, Z.; Wang, L.-W.; Liu, Y.; Alivisatos, A. P. PbS Nanoparticles Capped with Tetrathiafulvalenetetracarboxylate: Utlizing Energy Level Alignment for Efficient Carrier Transport. *ACS Nano* **2014**, *8*, 2532−2540.
(51) Crisp, R. W.; Schrauben, J. N.; Beard, M. C.; Luther, J. M.; Johnson, J. C. Coherent Exciton Delocalization in Strongly Coupled Quantum Dot Arrays. *Nano Lett.* **2013**, *13*, 4862−4869.
(52) Kaushik, A. P.; Lukose, B.; Clancy, P. The Role of Shape on Electronic Structure and Charge Transport in Faceted PbSe Nanocrystals. *ACS Nano* **2014**, *8*, 2302−2317.
(53) Prasittichai, C.; Avila, J. R.; Farha, O. K.; Hupp, J. T. Systematic Modulation of Quantum (Electron) Tunneling Behavior by Atomic Layer Deposition on Nanoparticulate SnO_2 and TiO_2 Photoanodes. *J. Am. Chem. Soc.* **2013**, *135*, 16328−16331.
(54) Rose, V.; Franchy, R. The Band Gap of Ultrathin Amorphous and Well-Ordered Al_2O_3 Films on CoAl(100) Measured by Scanning Tunneling Spectroscopy. *J. Appl. Phys.* **2009**, *105*, 07C902.